

these ions were implanted into insulators (ionic crystals and silicate glasses) to produce characteristic optical absorption band of implanted metal colloids. At that time these absorption bands were described in terms of optical scattering theory of metal colloids. Current terminology now favours the use "nanoparticles" to emphasize the more modern aspects of the processes. Later developments have expanded from the metal implants to the use of many ions and the active formation of compounds, including metal alloys and totally different composition precipitate inclusions [7]. Despite these steady advantages in the use of ion implantation for nanoparticle synthesis, there have not yet emerged clear mechanisms which provide precisely controlled particles sizes and depth distributions. Latter has a certain drawback which is the statistically nonuniform depth of penetration of implanted ions into a material [10,11]. This leads to a wide size distribution of synthesized nanoparticles not only in the plane parallel to the irradiated surface but also to a great extent over the depth of the sample [7,12,13]. Dispersion of nanoparticles with respect to sizes leads to a broadening of the SPR optical absorption band accompanied by a decrease in its intensity [4]. This is also attributable to the dependence of the SPR spectral position on the particle size, *i.e.* the absorption spectrum in real sample is a superposition of several overlapping less intense bands that correspond to particles of various sizes. The concern of the modern task is to increase the uniformity of the size distribution of metal nanoparticles synthesized by ion implantation using an approach based on the combination of high-power nanosecond pulse laser annealing with sequential furnace one. Experience gained from using the laser annealing techniques for various purposes allowed metal nanoparticles to be modified in various solid state dielectrics.

In general, the interaction of the high-power laser pulses with dielectrics containing metal nanoparticles for modification of their optical properties has been the subject of intense investigation for the last few years. This interest was conditioned by both a development of microelectronics based on composites with nanoparticles and also by a need for a fundamental understanding of the influence of high-power light on properties of the non-uniform composite media. In particular, such researches are focused on changes of the shape, the size, the size distribution, and the structure of the nanoparticles. Table 1 presents the data, compiled from available publications [14-38], on the types of metal nanoparticles in various matrixes and laser condi-

tions for their changes. As it follows from Table 1, composite materials made by ion implantation can be successfully modified depending on the laser wavelength, the power density or the pulse length. For example, Nd:YAG laser irradiation in the visible and near-IR region converts implanted spherical titanium silicide particles into ellipsoidal ones in silica and soda-lime glass [38]. Also, there are changes of the internal crystallographic structure of implanted iron particles after ruby laser (690 nm) treatment [15].

The main feature of most experiments described in Table1 is that the laser light was applied directly in the spectral region of the transparency of the dielectric matrix, and consequently, the intense laser pulses were primarily absorbed by the metal particles. In contrast to this case, a new approach for annealing was demonstrated by Wood *et al.* [23] in 1993, when float glass with silver particles was irradiated by a laser light at wavelengths of glass absorption in the ultraviolet region. When applying high-power excimer ArF (193 nm) laser pulses, a decrease of the reflectance intensity of composite samples was observed. It was suggested that the implanted silver particles in glass can be dissolved and the glass matrix can be modified to be a new metastable glass phase enriched by silver. If this suggestion is correct, the new phase can be destabilized to precipitate out the new silver particles in a controlled fashion by furnace. In reality, this new technique gives a variety of possibilities for controlled change of optical properties of implanted dielectrics, as suggested for the case of the combined laser annealing of float glass implanted with metal ions [27]. However, a number of questions regarding mechanisms of such modifications and interactions with high-power excimer laser light with non-uniform composite materials are now just starting to be understood. The literature in this field is expanding rapidly and the references cited here are mostly limited to amorphous dielectrics. However, with a rapid growth in the range of potential applications there is a much wider interest in target materials and types of inclusions.

2. INTERACTION OF HIGH-POWER EXCIMER-LASER PULSES WITH SODA-LIME SILICATE GLASS CONTAINING ION IMPLANTED SILVER NANOPARTICLES

Lets start with short characterisation of glasses with implanted nanoparticles. As it was mentioned in the introduction, low energy implantation of metal ions,

Table. Laser annealing of metal nanoparticles in solid state dielectric matrix (ASG - aluminosilicate glass, SLSG – soda-lime silicate glass).

<i>Metal</i>	<i>Matrix</i>	<i>Method of synthesis</i>	<i>Laser parameters</i>	<i>Laser annealing</i>	<i>Main results of laser annealing</i>	<i>Authors</i>
K	MgO [100]	ion implantation	YAG (1000 nm) laser and thermal annealing pulse 10 mJ	irradiation close to $\tau = 20$ ns, energy per area of nanoparticles but of matrix transparency	exfoliation of the surface layer the SPS spectral with particles from sample	Rankin <i>et al.</i> 1992 [14]
K	MgO [100]	ion implantation and thermal annealing	N ₂ (350 nm) laser $\tau = 20$ ns energy per pulse 10 mJ	irradiation in spectral area of matrix transparency	there are no recognized changes in the sample	Rankin <i>et al.</i> 1992 [14]
α -Fe	SiO ₂ glass	ion implantation	Rubin (690 nm) laser $\tau=40$ ns, energy density 0.1 - 0.3 J/cm ²	irradiation in the are of matrix transparency	ordering of the crystal structure of the particles	Bukharaev <i>et al.</i> 1991 [15]
Cu	Al ₂ O ₃ crystal	ion implantation	KrF (248 nm) excimer laser, $\tau=25$ ns, 1 Hz energy density 0.3 J/cm ²	irradiation in the absorption bands of matrix	reduction of the particles size	Stepanov <i>et al.</i> 2001 [16]
Cu	SiO ₂ SLSG glasses	ion implantation	KrF (248 nm) excimer laser, $\tau=25$ ns, 1 Hz energy density 0,2-0.32 J/cm ² , 1-250 pulses	irradiation in the absorption bands of matrix	reduction of the particles size and oxidation of Cu particles	Stepanov <i>et al.</i> 2000 [17] 2002 [18]
Cu	Polymer	plasma polymerization and metal evaporation	Nd:YAG (1064 nm) laser in the cw mode, the power from 8.6 to 1.1 W	irradiation in spectral area of matrix transparency	changes of particle size and shape by coalescence	Stepanov and Hole. 2002 [19] Werner <i>et al.</i> 1994 [20] Heilmann <i>et al.</i> 1995 [21]
Ag	ASG glass	ion-exchange	Q-switched Nd:YAG (532 nm) laser, $\tau=10$ ns, 10 Hz, energy density 0.18 and 0.6 J/cm ² , up to 1000 pulses	irradiation close to the SPS spectral area of nanoparticles but of matrix transparency	photochromic effect – depletion of metallic particles by photoionization.	Akella <i>et al.</i> 1997 [22]

Ag	SiO ₂ glass	ion implantation	ArF (193 nm) excimer laser, 500 pulses, 10 Hz	irradiation in the absorption bands of matrix	a dissolution of particles into glass network or a separation particles into smaller ones	Wood <i>et al.</i> 1993 [23] Townsend and Olivares 1997 [24] Ferrari <i>et al.</i> 1995 [25] Gonella <i>et al.</i> 1996 [26]
Ag	SiO ₂ glass	co-evaporation metal and glass	Argon and krypton lasers (350 nm), power 0.24-1 W, 5 min	irradiation close to the SPS spectral area of nanoparticles	increasing of the particles size	
Ag	SiO ₂ SLSG glasses	ion-exchange	Q-switched Nd:YAG (532 and 1064 nm) laser, $\tau=10$ ns, 10 Hz, energy density 0.3 and 5.0 J/cm ²	irradiation close to the SPS spectral area of nanoparticles but	increasing of the particles size and formation of new ones	
Ag	SiO ₂ glass	ion implantation	Nd:YAG (532 nm) laser, energy density 0.075 and 0.1 J/cm ²	irradiation close to the SPS spectral area but	a dissolution of particles into glass or a separation particles into smaller ones	Townsend and Olivares 1997 [24]
Ag	SiO ₂ SLSG glasses	ion-exchange followed by ion irradiation	Q-switched Nd:YAG (532 and 1064 nm) laser, $\tau=10$ ns, 10 Hz, energy density 0.3 and 5.0 J/cm ²	irradiation close to the SPS spectral area of nanoparticles but	reduction of the particles size as fragmentation and formation of Ag ₂ O shells on Ag core	Gonella <i>et al.</i> 1996 [26]
Ag	SiO ₂ SLSG glasses	ion implantation	KrF (248 nm) excimer laser, $\tau=25$ ns, 1 Hz energy density 0.2-0.25 J/cm ² , 1-250 pulses	irradiation in the absorption bands of matrix	reduction of the particles size followed with regrowth new ones	Stepanov <i>et al.</i> 1998 [27] 2000 [17]
Ag	SLSG glasses	ion-exchange	Ti:sapphire (400 nm) laser, $\tau<150$ fs, 1 Hz pulse intensity 10 ¹¹ W/cm ² linear polarization	irradiation close to the SPS spectral area of nanoparticles but	changes of particle shape from spherical to ellipsoidal with an additional halo of small particles around the central one	Kaempfe <i>et al.</i> 1999 [28] 2000 [29] 2001 [30] Seifert <i>et al.</i> 2000 [31]
Ag	Polymer	plasma polymerization and metal evaporation	Nd:YAG (1064 nm) laser in the cw mode, power from 8,6 to 1,1 W	irradiation in spectral area of matrix transparency	changes of particle size and shape by coalescence	Werner <i>et al.</i> 1994 [20] Heilmann <i>et al.</i> 1995 [21]

Ag	Polymer	simultaneous plasma polymerization and metal evaporation	Ti:sapphire (400 nm) laser, $\tau < 150$ fs, 1 Hz, energy 100 - 700 mJ	irradiation close to the SPS spectral area of nanoparticles but of matrix transparency	changes of particle shape from irregular to spherical and to large size by coalescence and recrystallisation	Kaempfe <i>et al.</i> 2001 [32]
Au	Polymer	simultaneous plasma polymerization and metal evaporation	Argon (514 nm) laser power 5 W	irradiation close to the SPS spectral area of nanoparticles but of matrix transparency	changes of particle shape from irregular to spherical and to large size by coalescence and recrystallisation	Comita <i>et al.</i> 1994 [33]
Au	Polymer	simultaneous plasma polymerization and metal evaporation	Ti:sapphire (800 nm) laser, $\tau < 150$ fs, 1 Hz, energy 100 - 700 mJ	irradiation close to the SPS spectral area of nanoparticles but of matrix transparency	changes of particle shape from irregular to spherical and to large size by coalescence and recrystallisation	Kaempfe <i>et al.</i> 2001 [32]
Bi	α -SiO ₂ crystal	Ion implantation	KrF (248 nm) excimer laser, $\tau = 20$ ns, 10 Hz energy density 0.15 J/cm ²	irradiation in the absorption bands of matrix	formation of Bi ₂ O ₃ and removal of particles from the sample surface	Park <i>et al.</i> 1998 [34]
Er	Al ₂ O ₃ crystal	Ion implantation and thermal annealing air	ArF (193 nm) excimer laser, $\tau = 12$ ns, 1 or 5 Hz energy density 0.15-0.4 J/cm ²	irradiation in the absorption bands of matrix	a dissolution of particles into matrix network	Can <i>et al.</i> 1994 [35] 1995 [36] Townsend and Olivares 1997 [24]
AuCu	SiO ₂ glass	ion implantation and thermal annealing in gas H ₂ -Ar (5% H ₂)	KrF (248 nm) excimer laser, $\tau = 20$ ns energy density 1 J/cm ²	irradiation close to the SPS spectral area of nanoparticles but of matrix transparency	increasing of the alloy particles size	Battaglin <i>et al.</i> 2001 [37]
AuAg	SiO ₂ glass	ion implantation and thermal annealing in gas H ₂ -Ar (5% H ₂)	KrF (248 nm) excimer laser, $\tau = 20$ ns, energy density 1.3 J/cm ²	irradiation close to the SPS spectral area of nanoparticles but of matrix transparency	increasing of the alloy particles size	Battaglin <i>et al.</i> 2001 [37]
Ti ₂ Si	SiO ₂ SLSG glasses	ion-exchange	O-switched Nd:YAG (532 and 1064 nm) laser, $\tau = 10$ ns, 10 Hz, energy density 0.04 and 0.6 J/cm ²	irradiation in the are of matrix transparency	change of particle shape from spherical to ellipsoidal and increasing Ti in silicide particles	Battaglin <i>et al.</i> 1998 [38]

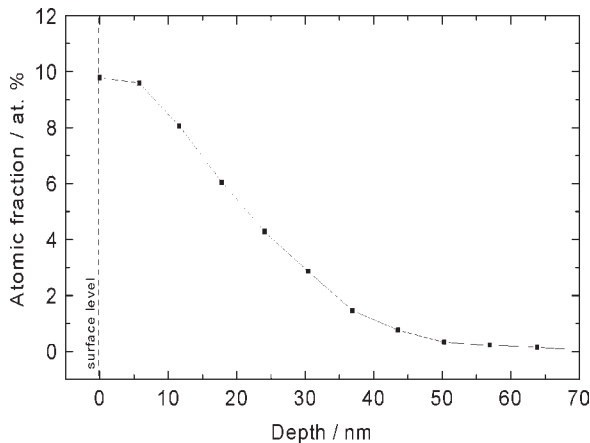


Fig. 1. The depth distribution of silver derived from the RBS spectrum for ion implantation with a dose of 7×10^{16} ion/cm² and energy of 60 keV into the soda-lime silicate glass [40].

as in our case, leads to a non-uniform ion distribution in the glass, which is different from the Gaussian profile traditionally predicted by statistical theory, primarily because of the effective sputtering from the substrate surface during the irradiation [39]. As seen in Fig. 1, the silver depth concentration in the soda-lime silicate glass (SLSG) derived from experimental Rutherford backscattering spectrometry (RBS) spattering shows a maximum near the implanted surface of the sample with some penetration to about 60–65 nm [40]. This characterises the implanted sample as a depth non-uniform metal/insulator object.

An excess of metal atoms in the glass, above the solubility limit, causes nucleation of the nanoparticles. As usually, the size distribution of metal nanoparticles appears here. In addition to this distribution in the implanted sample, there is a distribution of particles in the depth. Since the increase of metal concentration in the depth profile and the sputtering yield depend on implantation time, the metal particle nucleation and growth will also vary with both time and depth. It is obvious that, during the implantation, the size of the growing particles with depth is “proportional” to the metal filling factor, because they are both determined by the ion concentration profile. Consequently, according to Fig. 1, the large silver nanoparticles (or/and the higher filling factor) in the glass are close to the implanted surface, while small ones are located in the interior of the implant zone. Similar results were observed by electron microscopy experiments on Ag-ion implanted SLSG [12] and Co-ion implanted silica [41]. These features can be recognised in optical spectra of dielectrics with implanted nanoparticles. As

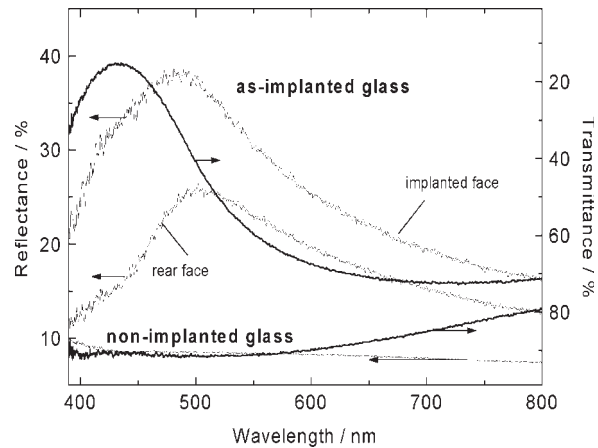


Fig. 2. Optical transmittance and reflectance of the silver implanted and original soda-lime silicate glass with a dose of 7×10^{16} ion/cm² and energy of 60 keV. Reflectance was measured from both the implanted and rear faces of the sample [13].

example, transmittance and reflectance data of the non-implanted and implanted glass are presented in Fig. 2. The transmission spectrum of implanted glass is maximised near 430 nm and the shape of the spectral curve is almost symmetrical. The reflectance spectra of the same sample are more complex and, although the transmission must be the same whether the glass is viewed from the implanted or the reverse face, the shapes of the reflectivity curves differ. Overlapping peaks of reflectance spectra measured from the implant face of the samples exhibit a shoulder at about 430 nm, on the side of a clearly determined maximum at 490 nm, whereas reflectivity from the rear face appears to have a simpler peak at longer wavelengths near 500 nm. The contrast between the spectrum available from transmittance and reflectance of the implanted glass is recognised as that coming from the non-uniform silver profile and size distribution of the nanoparticles in the implanted glass (Fig. 1). Since the distribution pattern is not symmetric, the reflectivity determined from the ion implanted and rear faces of the sample are different (Fig. 2), and the reflected intensity from a particular layer depends on their local absorption in the depth [13]. The atomic force microscope (AFM) images of the similar non-implanted and implanted samples are shown in Figs. 3 and 4 [11,27]. As seen from these figures, the implanted surface is smoother than those of the initial glass; and this is typical for irradiated glasses at similar conditions [42]. However, there are many hemispherical hills on this surface with an average diameter of approximately 100–150 nm. There are no such protrusions on the unimplanted

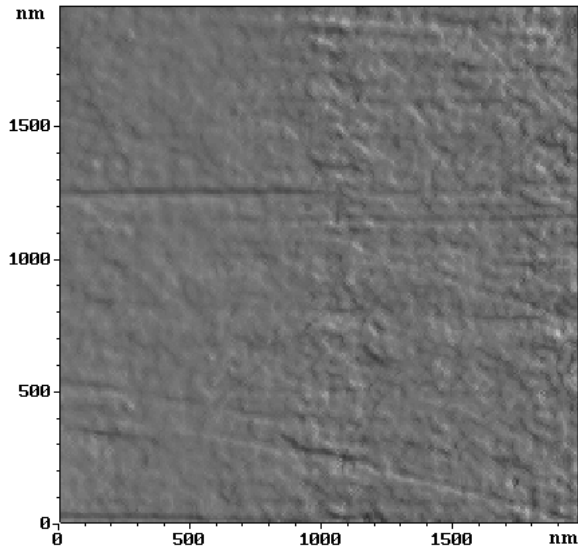


Fig. 3. An AFM image as a top view of the surface of SLSG before any treatment [11].

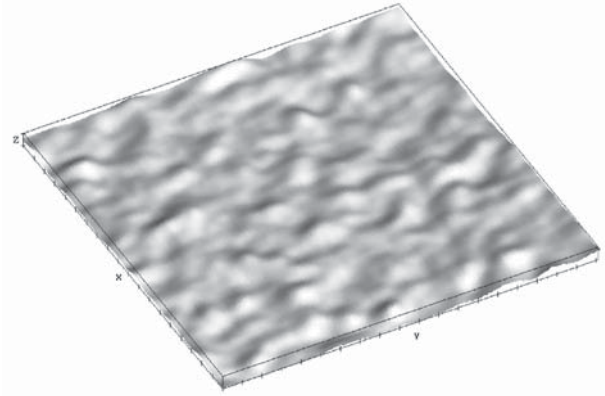


Fig. 4. An AFM image as a top view under lateral illumination of the surface of SLSG Ag-implanted with a dose of 7×10^{16} ion/cm² and energy of 60 keV. The step along the X and Y axes is 100 nm, and the step along the Z axis is 3 nm [27].

sample. The reason for the existence of surface hills is assumed to be from a sputtering of irradiated glass during implantation, which leads to unequal ejection of ions of different elements from the surface, exposing the synthesised nanoparticles in the sub-surface glass. The sputtered glass thickness is typically of the order of tens of nanometers for the present ion dose [43], and hence, the synthesised buried metal nanoparticles appear near to the glass surface in the implanted sample (Fig. 1).

Now let us consider the excimer laser pulse (25 ns) interaction with Ag-implanted SLSG. In general, the mechanisms of laser processing depend on the parameters of the laser beam and the physical-chemical properties of the material. The primary interactions between light and matter are non-thermal and lead to an electronic or vibrational photoexcitation. A prediction of how the laser processing will develop through thermal (photothermal) or non-thermal (photochemical) processes depends particularly on the values of the relaxation times involved. In laser processing for the present composite materials, the relevant excitations and conversions can be classified into those of the glass-substrate and the metal nanosize inclusions. Irradiation with a high power excimer laser at the wavelength of 248 nm (5 eV) couples directly through the spectral absorption of the SLSG, as the glass has a smaller energy bandgap (~ 3.5 eV). This creates electron-hole pairs by exciting an electron from the valence into the conduction band. In metals,

both conduction- and valence-band electrons may participate in laser excitations. The number and energy of absorbed photons immediately establishes the temperature rise in a laser-irradiated metal, whereas the number of valence-to-conduction-band excitations establishes the initial density of electron-hole pairs in an insulator [44]. In a metal, the time between electron-electron collisions is of the order of 10^{-14} to 10^{-13} s and electron-phonon relaxations are typically one to two orders of magnitude slower [45]. In non-metals, interband electronic excitations range from 10^{-12} to 10^{-6} s [44]. Overall, most of these times are short in comparison to the pulse duration (25 ns) of the laser described here, and so the laser energy can be viewed as releasing directly into a heating of the metal/glass composite. Thus, our following consideration of the laser treatments will be based on the effects of the thermalization processes.

Consequences of the excimer laser pulse with nanosecond pulse width and high beam intensity are heating, melting and/or vaporisation (ablation) of material on a time scale of nanoseconds to microseconds. The excimer laser treatment has been applied to many glasses [46,47], but there is less information on high-power pulse laser interaction with insulators containing metal nanoparticles. In the present case the energy density is lower than the value of the ablation threshold for the SLSG, which was determined to be about 5 J/cm^2 [47]. Also, the excimer laser is characterised by a UV-wavelength,

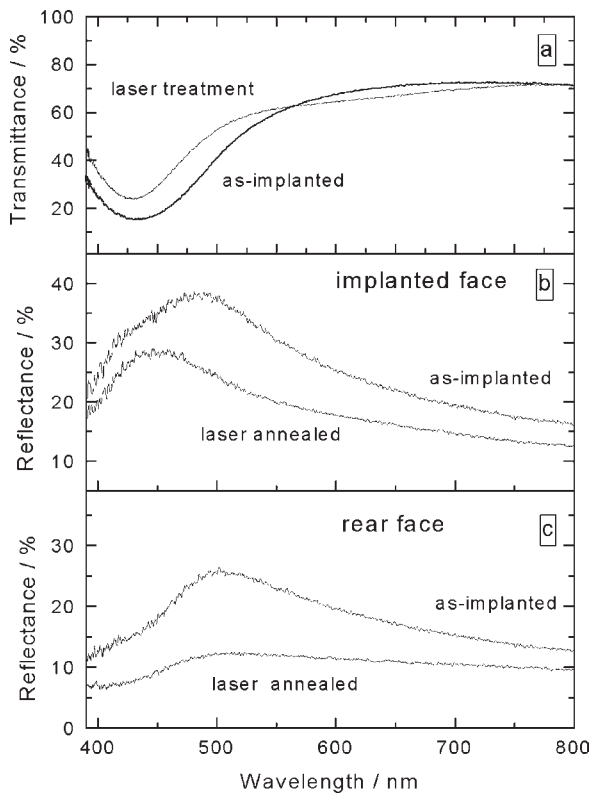


Fig. 5. Optical spectra of the soda-lime glass after silver implantation as in Fig. 2 and the implantation followed with laser treatment (0.2 J/cm^2): (a) transmittance; (b) reflectance measured from the implanted face; (c) reflectance measured from rear faces of the sample. [27].

which is much longer than the typical sizes of the nanoparticles formed by ion implantation. Hence, present metal/glass composites may be considered to be a homogeneous material for light propagation [4]. This is a simplification, which is true generally for low intensity light, but it gives an estimate of the optical penetration depth (α^{-1}) of the laser pulses into the composite material, where α is the linear absorption coefficient. An intense laser pulse is absorbed and released into heat into the surface SLSG layer of a thickness of α^{-1} , which is several microns [24], *i.e.*, deeper than the thickness of the implanted layer (Fig. 1).

The result of pulse laser treatment by 5 pulses of a KrF excimer laser with pulse length of 25 ns full-width at half-maximum at a wavelength of 248 nm with the total released energy of 0.2 J/cm^2 on the optical spectra of the Ag-implanted glass is presented in Fig. 5 [27]. Applied laser pulses did not change the reflectance and transmittance spectra of the non-implanted SLSG, but, for implanted sample, the location of the transmittance minimum

shifts slightly towards shorter wavelengths, and the transmittance in peak position increases from 16 to 23% (Fig. 4a). Remarkable change was found in the reflectance spectra, where in the case of the implanted surface, the peak of the overlapping bands shifts continuously from 490 to 450 nm with modifications in the shape of the envelope of the bands, which become narrower (Fig. 5b). The reflectance intensity falls from 38 to 27%. However, for reflectance from the rear face of the same sample (Fig. 5c), there is only a decrease in the intensity to a 13% maximum, which is at the same initial wavelength as in the implanted sample.

In practice, for the size evaluation of the metal nanoparticles the electromagnetic Mie theory [48,49] is often exploited, which is used also to describe qualitatively the laser modification of the metal-nanoparticle sizes in the implanted glass. However, Mie theory is properly applicable for highly separated and non-interacting particles only, *i.e.*, in the situation where the metal filling factor is extremely small (from 10^{-3} to 10^{-5}) [4]. As seen from Fig. 1 this value is much smaller than that in real implanted samples. For composite materials with large filling factors, and when electrodynamic particle-particle interactions are dominant, alternative effective-medium theories (Maxwell-Garnett, Bruggeman, *etc.*) should be considered [4]. According to these models, the measured optical intensities corresponding to the implanted glass (Figs. 2 and 5) are determined mainly by the near-surface layer, where there is the largest metal filling factor, and also the largest nanoparticles are present (Fig. 1). The smaller filling factors (and smaller nanoparticles) that exist at the other depths effectively influence only a smearing of the optical spectra. Moreover, consistent with effective-medium considerations, a decrease of the filling factor is accompanied by movement of the optical peak position to shorter wavelengths, as is shown in Fig. 5. Thus, a decrease of the filling factor in the composite resulted from laser treatment suggests there is a size reduction of all the silver nanoparticles, and the biggest nanoparticles are again localised near the SLSG surface. The difference between reflectance spectra from implanted and rear faces of laser treated sample (Fig. 4b,c) emphasises the existence of a non-symmetrical depth distribution of the silver nanoparticles as being similar to the distribution in the implanted sample.

RBS measurements (Fig. 6) show that the laser treatment causes a loss 30 % of the entire silver content in samples due to some evaporation of silver from the sample. Reduction of total silver concentration (filling factor) in the glass leads to de-

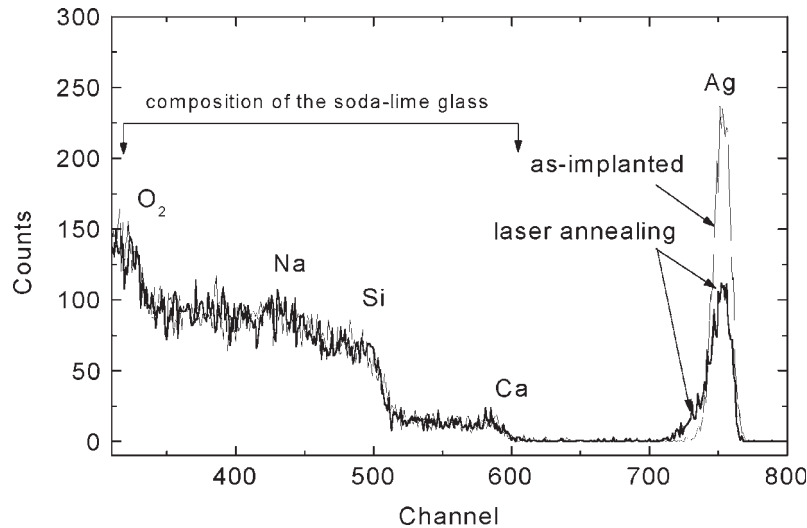


Fig. 6. The RBS spectrum for the Ag-implanted SLSG before and after laser treatment as in Fig. 5.

crease in the reflectance intensities measured both from implanted and rear side of sample (Fig. 5). These data are consistent with another observation of the thermal metal dissolution from the heated surface of the float glass with implanted silver nanoparticles after excimer laser irradiation [23], and with a later study of the silica glass with implanted bismuth particles [34]. At the same time, as seen in Fig. 6, the concentration peak position is not shifted, but the distribution of silver atoms is broadened compared to that of the as-implanted sample; this fact is explained by diffusion into the depth of the SLSG. All these processes decrease the filling factor. The assumption about the size-reduction is in agreement with AFM measurements of laser treated

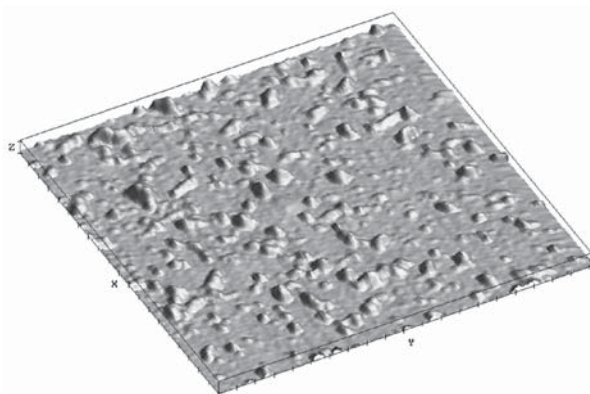


Fig. 7. An AFM image as a top view under lateral illumination of the surface of SLSG Ag-implanted with a dose of 7×10^{16} ion/cm² and energy of 60 keV followed with irradiation with an excimer laser (0.2 J/cm²) as in Fig. 5. The step along the X and Y axes is 100 nm, and the step along the Z axis is 40 nm [27].

samples. As shown in Fig 7 (notice an increased magnification of ten times in the direction perpendicular to plane of the figure), there are many clearly defined hills (believed to be silver particles) on the glass surface whose size is one order smaller compared to large hills on the implanted glass surface in Fig. 4. The silver accumulation effect on the laser-irradiated surface of glass is a result of implanted composite layer melting and some desorption of glass material under the laser pulses, which exposes the melted metal particles after their solidification. Hence, the first of the conclusions from the present data on excimer laser treatment of implanted glass is the reduction of the size of the silver nanoparticles, and second is the existence of some asymmetry in their depth distribution (Fig. 5b,c). To recognise the mechanisms by which the changes occur for strongly absorbed excimer laser pulses, the thermal propagation after the laser-irradiation must be taken into consideration. The laser heating is traditionally characterised by the heat diffusion length, $l(t) = (D \cdot t)^{1/2}$, where D is the heat diffusivity, and t is the laser pulse duration. In the present experiment with laser pulses of 25 ns, the heat propagation is approximately $l(t) = 115$ nm, that is shorter than the α^{-1} , i.e., the temperature rise is no longer controlled by the diffusion of the heat. However, the $l(t)$ surpasses the depth of the implanted silver nanoparticles. As was estimated earlier [24], temperature at the surface of laser treated soda-lime glass reaches values exceeding 700 °C which is equivalent to the SLSG melting temperature. Under these temperature conditions, the melting of the small silver particles is likely, because their melting

temperature is drastically decreased, for example, to ~ 400 °C for sizes < 30 nm, compared with the bulk metal melting temperature of 960 °C [50]. As was noticed above, the time scale of electronic relaxation and energy transfer to the lattice vibrations in the metal particles is several orders smaller than that in the surrounding glass medium. Therefore, during the interaction of the excimer laser pulse with the metal/glass composite, the silver nanoparticles are heated and melted more quickly than solidification of the melted glass can occur. Atomically dispersed silver released from nanoparticles enters into the glass melt, and immediately diffuse throughout all the heated thickness of the laser treated substrate. In principle, in time this could lead to a uniform metal distribution, where the silver atom concentration exceeds the solubility value in the solid glass. However, following glass solidification spreading from the depth to the surface, as heat from the laser pulse penetrates into the depth of the sample, the cooling part of the annealing cycle will stimulate new nucleation and regrowth of metal particles. In this case, the possibility of regrowth of metal particles will depend on competition between regrowth and the cooling speed of the moving solidification front, resulting in a new non-uniform size distribution of new metal nanoparticles over a depth scale similar to that after ion implantation. Obviously, under some conditions the metal particles may be dispersed into separate metal ions and/or into such small units that they can not display optical properties exhibited by nanoparticles. The present consideration of the melting of the metal nanoparticles is also suitable for a description of the reflectance modification discussed in previous article [23]. In alternative interpretations of the data in that article, the authors of [51] preferred to treat the data as evidence for an evaporation of metal atoms from the surface of nanoparticles, which resulted in shrinkage of the average size. Similarly, in paper [34], for case of the implanted bismuth nanoparticles in silica glass treated with a KrF excimer laser, the melting of the particles was completely ignored, though the melting point of the bismuth nanoparticles is very low (~ 140 °C for the size of 20 nm [52]), and primarily the feature was thought to be the thermal evaporation atoms from the particles. Evaporation is of course one of the thermal consequences from high power laser processing and leads to some ablation of the metal and film surface, and dissolution of metal inclusions on non-metal substrates; see for example, [51]. However, in the case of implanted composite material, metal nanoparticles are not only localised immediately at the glass surface, but also

extend into the depth of heated solid media. Hence, processes of atom evaporation from the nanoparticles will be very different from those limited to particles on the outer surface. Therefore the description of the size modification of the implanted metal nanoparticles based on a particle-melting approach seems reasonable. Thus, metal ion implantation in glass invariably results in a very wide distribution of nanoparticle sizes that vary with the depth. As firstly shown here, subsequent high power excimer laser pulse treatments of the ion implanted layer may be used to melt, and/or regrow, the metal nanoparticles within the insulator medium. Overall, this results in a tighter distribution of small particles. The laser treatments have slightly reduced, but not completely removed evidence for a non-symmetric depth distribution of the silver particles. The silver-insulator composite material is complex, and so a much wider range of laser pulse conditions, and more data on the cooling rates are required to fully model the changes in the size distributions which can occur.

3. MULTIPULSE LASER ANNEALING OF SODA-LIME SILICATE GLASS CONTAINING ION IMPLANTED SILVER NANOPARTICLES

Previous example of laser annealing were carried out only with pulses of the lower energy density ~ 0.2 J/cm², but the excimer laser gives the possibility of more powerful treatment of materials. The present description concentrates on experiments with KrF laser annealing (25 ns), employing a higher level of energy density per pulse (0.25 J/cm²) and a larger number of pulses until 250 at a repetition rate of 1 Hz to evaluate the modification of the metal-implanted glasses. The reflectance spectra for Ag-implanted SLSG for different numbers of pulses are shown in Figs. 8 and 9. All spectra of samples, including the annealed ones, are characterized by selective plasmon resonance bands determined by silver particles. As seen from this figure, approximately 50 pulses of the laser treatment initiates a decrease of reflectance intensity from 26 to 12 %. The fall in reflectance following laser annealing is qualitatively consistent with previous example for the case of the lower pulse fluence of 0.2 J/cm². It is again suggested there that either the metal nanoparticles were dispersed into atoms, or the large particles were separated into such small units that do not interact as particles. The salient feature of the present data is a remarkable increase of reflectance when more than 50 pulses are applied. After about

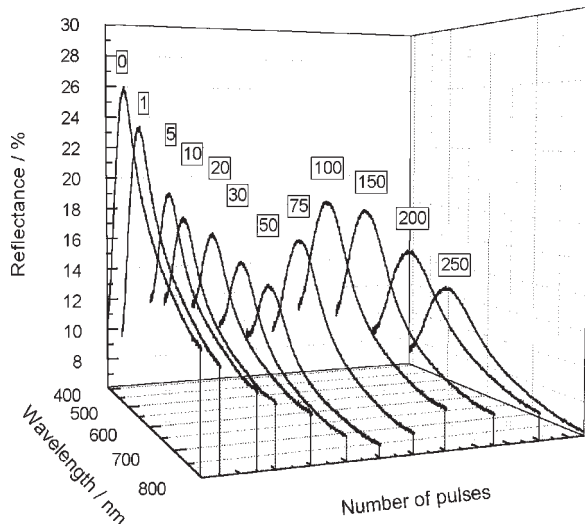


Fig. 8. Reflectance of Ag-implanted soda-lime silicate glass after a dose of 4×10^{16} ion/cm² treated with various numbers of excimer laser pulses (0.25 J/cm²) [10].

100 pulses, where the reflectance reaches a maximum value, the intensities decrease again. Such an intensity increase, with dependence on number laser pulses, has not been detected before, for either metal implanted dielectrics, as seen in already mentioned articles, or different composites of insulators with metal nanoparticles, for example, particles in aqueous solutions [54] or in melted photochromic aluminosilicate glass [22]. Plasmon excitations in small metal particles are well described by Mie scattering theory for electromagnetic waves (Mie 1908). According to this approach, increase in the size of metal nanoparticles is accompanied by movement of the spectral peak of the optical resonance to longer wavelengths. To evaluate the size change of implanted silver nanoparticles after laser treatment, in Fig. 8 some selective spectra of reflectance from Fig. 1 are presented in a plane view. It should be mentioned that the observed spectra are presented as a superposition of plasmon bands influenced from all size-distributed particles in the sample, and so the exact determination of the particle size from the width of spectral bands is not suited. As seen in Fig. 8 the reduction of reflectance during of first 50 pulses is accompanied by moving of peak position to shorter wavelength. These changes induced by laser treatment suggest there is reduction of the nanoparticles. However, further increase of number of laser pulses shifts the overall plasmon bands, which are broadening, to red spectral region that seems appearance a wide size distribution of silver particles.

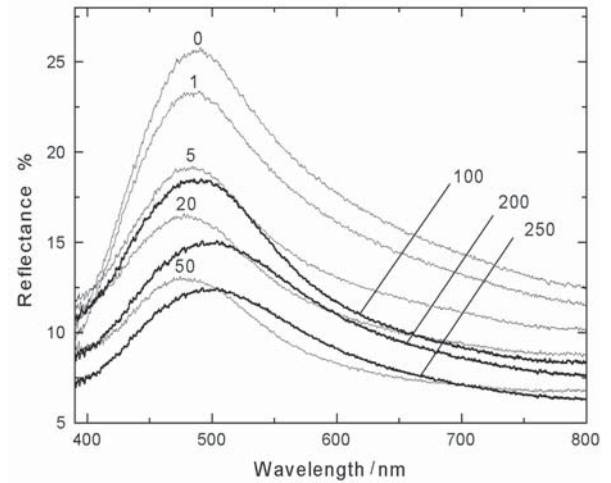


Fig. 9. Selected reflectance spectra from Fig. 7 presented in plane view [53].

RBS data show that laser treatment modifies the silver profile in the glass by lowering of the local concentration in the maximum and by inward diffusion in proportion to the number of pulses. Measurable changes of profiles appear only if more than 50 pulses are applied. For a fewer number of laser pulses, the RBS curves are very similar and symmetrical. As an example, in Fig. 10 the RBS spectra for the cases of the Ag-implanted sample and those corresponding to two anneals with 50 and 100 pulses are presented. The concentration peak po-

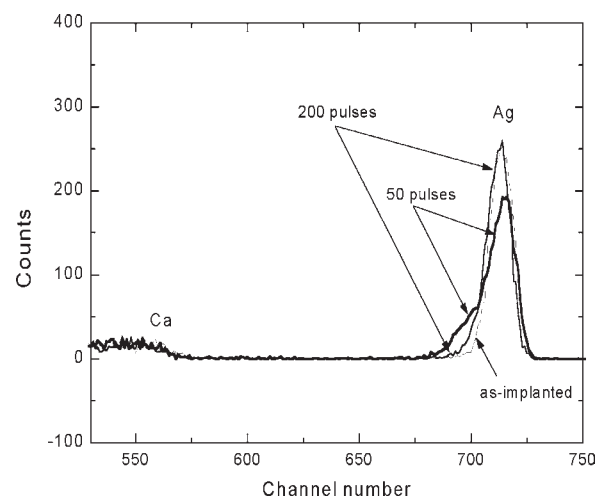


Fig. 10. RBS data for Ag-implanted soda-lime silicate glass after a dose of 4×10^{16} ion/cm² treated with various numbers of excimer laser pulses (0.25 J/cm²) [10,53].

sition was not shifted, but the distribution of silver atoms is broadened and is explained by diffusion into the depth of the SLSG. According to the position of the concentration tail in RBS spectrum (Fig. 10) and the data on silver profile depth in implanted SLSG [13], the penetration depth of in the sample is assumed to be approximately 60 nm. Inward silver migration in the sample during annealing shows that there is heating of the treated sample surface, and as a consequence the diffusional mobility of metal atoms in the glass is increased.

Thus, in the present example of high-energy density laser pulses, the average temperature of the sample slowly rises after several pulses, reducing the cooling effect. The continuing heating of the glass with high concentration of silver atoms leads to a new nucleation stage, and this allows regrowth of metal particles to occur, that immediately results in the increased reflectance (Fig. 8). Notice, however, that the size and depth distributions may have been altered. Laser treatment with more than 150 pulses eventually raises the sample to such a high temperature that the fast metal diffusion lowers the silver concentration and prevents further particle nucleation. Metal-ion implantation in glass invariably results in a very wide distribution of nanoparticle sizes that vary with the depth. As seen from present data, subsequent high-power excimer laser treatments with high number of pulses of the ion implanted layer may be used to melt, and/or regrow, the metal nanoparticles within the insulator medium. This is a new multipulse approach for particle modifications and is different from previous ones, which suggested the use of laser annealing, as a first step for a total dissolution of implanted metal particles, and regrowth then by second treatment in a furnace or with low-energy laser irradiation [55].

4. COMBINED LASER AND THERMAL ANNEALING OF SILICATE GLASS WITH SILVER NANOPARTICLES

The concern of the present part of review is to describe how to increase the uniformity of the size distribution of metal nanoparticles synthesized by ion implantation using an approach based on the combination of high-power pulse laser annealing with sequential furnace one [55]. As example, consider a silicate glass implanted by 60 keV Ag⁺ ions with a dose of $3 \cdot 10^{16}$ ion/cm². The implanted glasses were irradiated by 5 pulses of a KrF excimer laser with pulse length of 25 ns full-width at half-maximum at a wavelength of 248 nm with the total released energy being kept equal to 0.2 J/cm². After

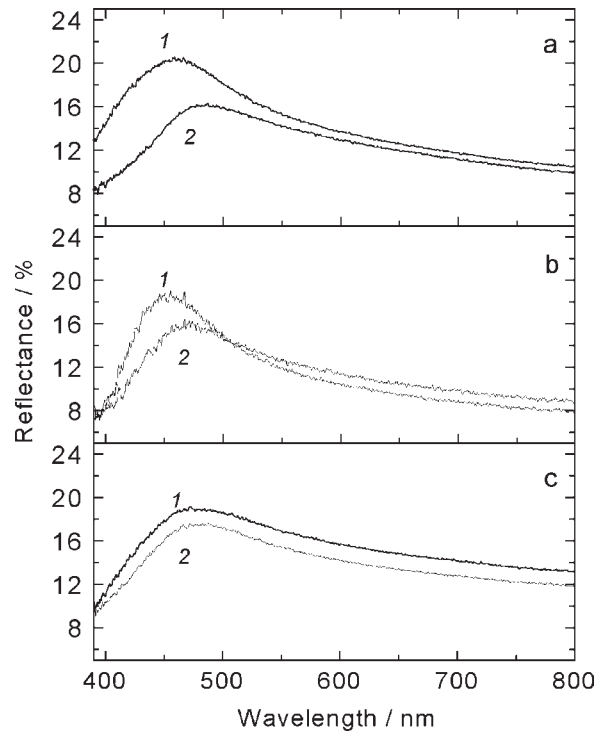


Fig. 11. Optical reflectance measured from the implanted side (1) and from the rear side (2) for the samples after ion implantation (a), implantation followed with laser treatment (b), and implantation with the sequential laser and thermal annealing (c).

laser treatment, the samples were annealed in a furnace according to the conventional procedure at a temperature of 350 °C for 1 h in air. As a control instrument the Mie theory [48,49] can be applied for the modeling of optical spectra. This theory allows the calculation of an optical extinction cross section σ_{ext} for a single isolated nanoparticle embedded into different media. Simulated optical spectra in present here are shown as spectral dependencies of σ_{ext} using the well-known Mie equations. Dielectric functions of Ag and Ag₂O nanostructured materials for calculations are taken from [56] and [57], respectively.

As it was shown earlier the nonuniformity in size distribution of metal particles over the depth leads to dissimilar absorption and reflection of layers containing nanoparticles different in size. This was observed by the pronounced discrepancy between the reflection spectra recorded on the implanted side and rear one. Similar a spectral discrepancy is recorded in the present work. From Fig. 11a it is seen that the reflection recorded from the implanted side of the sample is characterized by a broad band with a maximum at 460 nm while the reflection maxi-

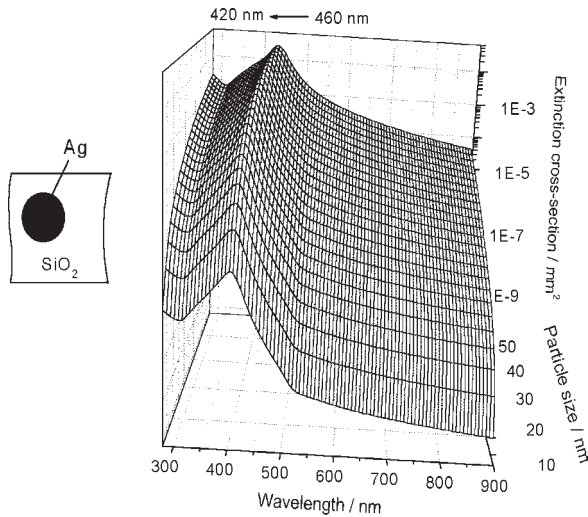


Fig. 12. Calculated extinction spectra of Ag nanoparticles in the glass as a function of the size.

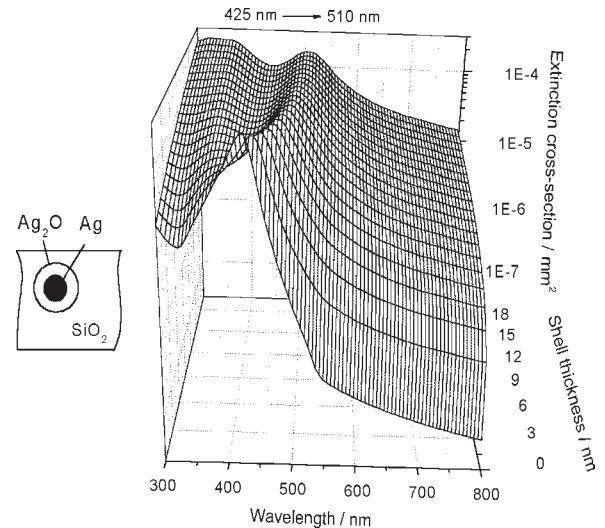


Fig. 13. Calculated extinction spectra of Ag nanoparticles with Ag_2O shell in the glass depending on the shell thickness. The core size is constant and equal to 10 nm.

mum is near 485 nm for the rear side. Thus, there is a possibility to use an optical spectroscopy for registration of the particles size uniformity in a sample. Optical reflection spectra of the implanted samples after the pulsed laser annealing are presented in Fig. 1b. It is seen that, after laser irradiation, the spectra corresponding to reflection from both surfaces of the sample undergo the changes. The spectrum after the laser annealing is characterized by a narrower reflection band compared to the spectrum of the as-implanted sample measured on the implanted surface (curve 1 in Fig. 11a and 11b). The reflection maximum shifts toward the short wavelengths up to 450 nm. A similar shift of the reflection band is also observed for the spectrum recorded on the rear side, with the maximum turning out to be at 475 nm. However, despite the coherent shift of the bands toward UV region, the pronounced spectral difference between different sides of the sample still persists, thus characterising the available nonuniform size distribution of the silver nanoparticles over the depth.

In Fig. 12 modeled Mie extinction spectra of silver nanoparticles in the glass environment with dependence on a particle size from 5 to 50 nm, which corresponds to typical values [7], are presented. As seen in this figure, the decrease in the nanoparticle size is accompanied by the movement of the SPR peak to shorter wavelengths with reduction of the intensity. This peak shift is caused by the phase retardation of the electromagnetic waves and the influence of higher multipoles [49]. Com-

parison of the calculation with the experimental data (Fig. 11) also suggests that the laser treatment of the glass with Ag nanoparticles stimulates a decrease of their size. As was mentioned before, this reduction in size is explained by the fact that laser emission in the spectral region of glass absorption causes heating-up and melting of the near-surface layer within only several nanoseconds. With laser heating-up of the glass matrix to temperature higher than the melting point of metal nanoparticles, the particles undergo melting that results in decrease of their sizes up to complete dissociation. On the other hand, in the experiments with Nd:YAG laser treatment of Ag implanted nanoparticles in silicate glasses [26], the oxidation of the metal particle was assumed to be a reason for the degradation of optical extinction of the composites. To check such a possibility in our case, the extinction spectra of core Ag particles with Ag_2O shells in the glass were calculated using "recursion formalism" [58]. In this modeling, the diameter of the metal core was taken to be constant, equal to 10 nm and the thickness of the shell was varied monotonically from 0 to 10 nm (Fig. 13). It is shown that the increase in thickness of the shell shifts the extinction peak to longer wavelengths and the intensity of the SPR band decreases. This is contrasted to the current observations (Fig. 11). Thus, the calculations allow one to infer that after the excimer laser annealing of the implanted glass, a decrease in the Ag particle size is more probable than the particle oxidation. Hence, in laser treatment, conditions are realized under

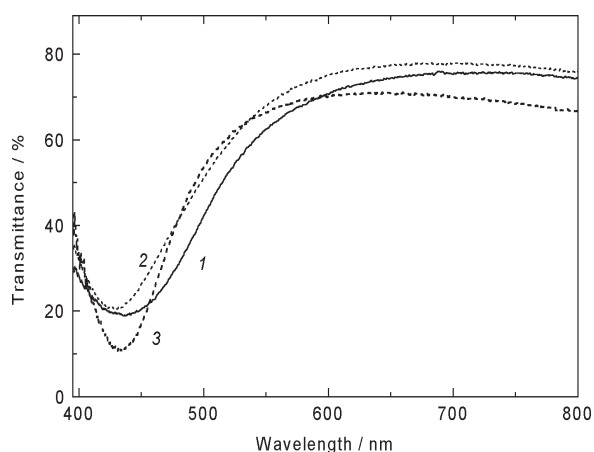


Fig. 14. Transmittance of the glass after ion implantation (1), implantation followed with laser treatment (2), and implantation with the sequential laser and thermal annealing (3).

which the near-surface layer of the glass turns out to be saturated with silver atoms and their aggregates which can serve as nuclei for synthesis of an ensemble of new nanoparticles characterized by more uniform size distribution. For this purpose, after the ion implantation and pulsed laser irradiation the samples can be furnace annealed.

Optical reflectance spectra of the samples after the implantation, laser and furnace annealing are presented in Fig. 11c. The distinctive feature of the optical spectra recorded both on the implanted and rear sides is the exact coincidence of the maxima positions at 475 nm and the spectral shapes. A slight difference in the intensities of the bands can be attributed to the thickness of the glass backing and associated light losses in recording the reflection on the side of the backing. The observed similarity of the spectra is indicative of the fact that, after the sequential pulsed laser irradiation and thermal annealing, the composite layer with the uniform size distribution of the metal nanoparticles over the depth is formed. This effect is explained by the increase of the diffusional mobility of silver atoms during the annealing of the sample in a furnace, which is accompanied by enlargement of metal nanoparticles with simultaneous averaging of their sizes practically throughout the entire implanted layer.

Narrowing of the size distribution function of the metal nanoparticles should lead to an increase in the absorption coefficient near the SPR maximum, that is shown in Fig. 14. From the presented optical transmission spectra it is seen that, for the as-im-

planted sample, the intensity of the band corresponding to absorption caused by silver nanoparticles is markedly lower than that in the sample after the sequential laser and furnace treatment. This increase of absorption does not allow one to suggest that silver particles are oxidized by annealing in furnace. It was already mentioned that the increase of the linear absorption of glasses with metal nanoparticles as a consequence of SPR inevitably causes an increase of the third order susceptibility of the material. Moreover, from Fig. 14 it is seen that the maximum of the transmission band of the composite glass after the combined treatment lies between the more longwave maximum of the implanted glass and the more shortwave maximum corresponding to the glass after the implantation and laser irradiation. According to the Mie theory, for metal nanoparticles with a diameter less than $\lambda/20$, where λ is the wavelength of light, the position of the absorption maximum of the material is determined by the mean size of nanoparticles in it. Consequently, the mean size of Ag nanoparticles in the glass after final heat treatment can reach, according to our estimations, 5-10 nm.

Using silver ion implantation into the silicate glass in combination with high-power pulsed irradiation by an excimer laser (in the absorption band of the glass matrix) and furnace annealing, one can create composite materials characterized by a high filling factor and uniform size distribution of the metal nanoparticles throughout the entire implanted layer of the material. The approach developed makes it possible to fabricate more advanced elements of nonlinear optics and also to control their characteristics by simple methods of optical spectroscopy.

ACKNOWLEDGMENTS

The author is grateful to the Alexander von Humboldt Foundation (Germany) for financial supports and also to the Russian Government Support of leading scientific schools (No. HШ 1904.2003.2).

REFERENCES

- [1] R.F. Haglund, Jr. // *Mater. Sci. Eng. A* **253** (1998) 275.
- [2] G.I. Stegeman and R.H. Stolen // *J. Opt. Soc. Am. B* **6** (1989) 652.
- [3] D. Ricard, P. Roussignol and C. Flytzanis // *Opt. Lett.* **10** (1985) 511.
- [4] U. Kreibig and M. Vollmer, *Optical properties of metal clusters* (Springer-Verlag, Berlin, 1995).

- [5] L. Minyung, S.K. Taek and S.C. Young // *J. Non-Cryst. Sol.* **211** (1997) 143.
- [6] R.F. Haglund, Jr., In: *Handbook of optical properties. Volume II. Optics of small particles, interfaces and surfaces*, ed. by R.E. Hummel and P. Wissmann (CRC Press: New York, 1998) p. 191.
- [7] P.D. Townsend, P.J. Chandler and L. Zhang, *Optical Effects of Ion Implantation* (University Press, Cambridge, 1994).
- [8] J. Davenas, A. Perez, P. Thevenard and C.H.S Dupuy // *Phys. Stat. Sol. A* **19** (1973) 679.
- [9] G.W. Arnold // *J. Appl. Phys.* **46** (1975) 4466.
- [10] A.L. Stepanov, V.A. Zhikharev, D.E. Hole, P.D. Townsend and I.B. Khaibullin // *Nucl. Instr. Meth. B* **166/167** (2000) 26.
- [11] A.L. Stepanov, V.A. Zhikharev and I.B. Khaibullin // *Phys. Sol. State* **43** (2001) 766.
- [12] L.C. Nistor, J. van Landuyt, J.B. Barton, D.E. Hole, N.D. Skelland and P.D. Townsend // *J. Non-Cryst. Solids.* **162** (1993) 217.
- [13] A.L. Stepanov, D.E. Hole and P.D. Townsend // *Nucl. Instr. Meth. B* **161/163** (2000) 913.
- [14] J. Rankin, P. Thevenard, L.J. Romana, L.A. Boatner, C.W. White, C.J. McHargue and L.L. Horton // *Surf. Coat. Technol.* **51** (1992) 471.
- [15] A.A. Bukharaev, A.V. Kazakov, R.A. Manapov and I.B. Khaibullin // *Sov. Phys. Solid State* **33** (1991) 578.
- [16] A.L. Stepanov, U. Kreibig, D.E. Hole, R.I. Khaibullin, I.B. Khaibullin and V.N. Popok // *Nucl. Instr. Meth. B* **178** (2001) 120.
- [17] A.L. Stepanov, D.E. Hole and P.D. Townsend // *Nucl. Instr. Meth. B* **166/167** (2000) 882.
- [18] A.L. Stepanov, D.E. Hole and P.D. Townsend // *Nucl. Instr. Meth. B* **191** (2002) 468.
- [19] A.L. Stepanov D.E. and Hole // *Surf. Coat. Tech.* **158/159** (2002) 526.
- [20] J. Werner, A. Heilmann and O. Stenzel // *Int. J. Electronics* **77** (1994) 945.
- [21] A. Heilmann, J. Werner, F. Homilius and F. Müller // *J. Adhesion Sci. Technol.* **9** (1995) 1181.
- [22] A. Akella, T. Honda, A.Y Liu and L. Hesselink // *Opt. Lett.* **22** (1997) 967.
- [23] R.W. Wood, P.D. Townsend, N.D. Skelland, D.E. Hole, J. Barton and C.N. Afonso // *J. Appl. Phys.* **74** (1993) 5754.
- [24] P.D. Townsend and J. Olivares // *Appl. Surf. Sci.* **109/110** (1997) 275.
- [25] M. Ferrari, L.M. Gratton, A. Maddalena, M. Montagna and C. Tosello // *J. Non.-Cryst. Solids* **191** (1995) 101.
- [26] F. Gonella, G. Mattei, P. Mazzoldi, E. Cattaruzza, G.W. Arnold, G. Battaglin, P. Calvelli, R. Polloni, R. Bertoncetto and R.H. Haglund, Jr. // *Appl. Phys. Lett.* **69** (1996) 3101.
- [27] A.L. Stepanov, D.E. Hole, A.A. Bukharaev, P.D. Townsend and N.I. Nurgazizov // *Appl. Sur. Sci.* **136** (1998) 298.
- [28] M. Kaempfe, T. Rainer, K.-J. Berg, G. Seifert and H. Graener // *Appl. Phys. Lett.* **74** (1999) 1200.
- [29] M. Kaempfe, H. Hofmeister, S. Hopfe, G. Seifert and H. Graener // *J. Phys. Chem. B* **104** (2000) 11847.
- [30] M. Kaempfe, G. Seifert, K.-J. Berg, H. Hofmeister and H. Graener // *Eur. Phys. J. D* **16** (2001) 237.
- [31] G. Seifert, M. Kaempfe, K.-J. Berg and H. Graener // *Appl. Phys. B* **71** (2000) 795.
- [32] M. Kaempfe, H. Graener, A. Kiesow and A. Heilmann // *Appl. Phys. Lett.* **79** (2001) 1876.
- [33] P.B. Comita, E. Kay, R. Zhang and W. Jacob // *Appl. Surf. Sci.* **79/80** (1994) 196.
- [34] S.Y. Park, T. Isobe, M. Senna, R.A. Weeks and R.A. Zuhr // *Appl. Phys. Lett.* **73** (1998) 2687.
- [35] N. Can, P.D. Townsend and D.E. Hole // *Appl. Phys. Lett.* **65** (1994) 1871.
- [36] N. Can, P.D. Townsend, D.E. Hole, H.V. Snelling, J.M. Ballesteros and C.N. Afonso // *J. Appl. Phys.* **78** (1995) 6737.
- [37] G. Battaglin, E. Cattaruzza, C. de Julian Fernandez, G. De Marchi, F. Gonella, G. Mattei, C. Maurizio, P. Mazzoldi, A. Miotello, C. Sada, and F. D'Acapito // *Nucl. Instr. Meth. B* **175/177** (2001) 410.
- [38] G. Battaglin, E. Borsella, E. Cattaruzza, F. Gonella, R.F. Haglund, Jr., G. Mattei, P. Mazzoldi, D.H. Osborne, Jr. and R. Polloni // *Nucl. Instr. Meth. B* **141** (1998) 274.
- [39] P.D. Townsend, J.C. Kelly and N.E.W. Hartley, *Ion implantation, sputtering, and their applications* (Academic Press, London, 1996).
- [40] A.L. Stepanov, D.E. Hole and P.D. Townsend // *J. Non.-Cryst. Solids* **244** (1999) 275.
- [41] O. Cintora-González, D. Muller, C. Estournès, M. Richard-Plouet, R. Poinot,

- J.J. Grob and J. Guille // *Nucl. Instr. Meth. B* **178** (2001) 144.
- [42] A.A. Bukharaev, V.M. Janduganov, E.A. Samarsky and N.V. Berdunov // *Appl. Surf. Sci.* **103** (1996) 1198.
- [43] D.E. Hole, A.L. Stepanov and P.D. Townsend // *Nucl. Instr. Meth. B* **148** (1998) 1054.
- [44] D. Bäuerle, *Laser processing and chemistry* (Springer-Verlag, Berlin, 1996).
- [45] J.Y. Bigot, J.C. Merle, O Cregut and A. Daunois // *Phys. Rev. Lett.* **75** (1995) 4702.
- [46] K. Arai, H. Imai, H. Hosono, Y. Abe and H. Imagawa // *Appl. Phys. Lett.* **53** (1988) 1891.
- [47] C. Buerhop, B. Blumenthal, R. Weissmann, N. Lutz and S. Biermann // *Appl. Surf. Sci.* **46** (1990) 430.
- [48] G. Mie // *Ann. Phys.* **25** (1908) 377.
- [49] C.F. Bohren and D.R. Huffman, *Absorption and scattering of light by small particles* (John Wiley & Sons, New York, 1983).
- [50] T. Castro, R. Reifenberger, E. Choi and R.P. Andres // *Phys. Rev. B* **42** (1990) 8548.
- [51] J. Bosbach, D. Martin, F. Stietz, T. Wenzel and F. Träger // *Appl. Phys. Lett.* **74** (1999) 2605.
- [52] H. Itoigawa, T. Kamiyama and Y. Nakamura // *J. Non-Cryst. Solids* **210** (1997) 95.
- [53] A.L. Stepanov and D.E. Hole // *Phil. Mag. Lett* **82** (2002) 149.
- [54] A. Takami, H. Yamada, K. Nakano and S. Koda // *Jap. J. Appl. Phys.* **35** (1996) L781.
- [55] A.L. Stepanov, D.E. Hole and P.D. Townsend // *Nucl. Instr. Meth. B* **149** (1999) 89.
- [56] M. Quinten // *Z. Phys. B* **1001** (1996) 211.
- [57] L.A.A. Pettersson and P.G. Snyder // *Thin Solid Films* **270** (1995) 69.